AGU PUBLICATIONS

JGR

Journal of Geophysical Research: Atmospheres

RESEARCH ARTICLE
10.1002/2017JD026565

Key Points:
- Certain errors shown in SCM simulated clouds and precipitation are due to the lack of spatial variability with the domain-mean large-scale forcing
- The gridded large-scale forcing data describe the spatial variability and help SCMs better capture cloud systems
- Applications of the gridded forcing data in testing scale-aware parameterizations are presented

Correspondence to:
S. Tang,
tang32@llnl.gov

Citation:
Tang, S., M. Zhang, and S. Xie (2017), Investigating the dependence of SCM simulated precipitation and clouds on the spatial scale of large-scale forcing at SGP, *J. Geophys. Res. Atmos.*, *122*, 8724–8738, doi:10.1002/2017JD026565.

Received 26 JAN 2017
Accepted 3 AUG 2017
Accepted article online 5 AUG 2017
Published online 19 AUG 2017

Investigating the dependence of SCM simulated precipitation and clouds on the spatial scale of large-scale forcing at SGP

Shuaiqi Tang[1], Minghua Zhang[2], and Shaocheng Xie[1]

[1]Lawrence Livermore National Laboratory, Livermore, California, USA, [2]School of Marine and Atmospheric Sciences, Stony Brook University, Stony Brook, New York, USA

Abstract Large-scale forcing data, such as vertical velocity and advective tendencies, are required to drive single-column models (SCMs), cloud-resolving models, and large-eddy simulations. Previous studies suggest that some errors of these model simulations could be attributed to the lack of spatial variability in the specified domain-mean large-scale forcing. This study investigates the spatial variability of the forcing and explores its impact on SCM simulated precipitation and clouds. A gridded large-scale forcing data during the March 2000 Cloud Intensive Operational Period at the Atmospheric Radiation Measurement program's Southern Great Plains site is used for analysis and to drive the single-column version of the Community Atmospheric Model Version 5 (SCAM5). When the gridded forcing data show large spatial variability, such as during a frontal passage, SCAM5 with the domain-mean forcing is not able to capture the convective systems that are partly located in the domain or that only occupy part of the domain. This problem has been largely reduced by using the gridded forcing data, which allows running SCAM5 in each subcolumn and then averaging the results within the domain. This is because the subcolumns have a better chance to capture the timing of the frontal propagation and the small-scale systems. Other potential uses of the gridded forcing data, such as understanding and testing scale-aware parameterizations, are also discussed.

1. Introduction

Single-column models (SCMs) and cloud-resolving models (CRMs) have been widely used as the modeling tools to evaluate and improve physical parameterizations in climate models for more than two decades [*Randall et al*., 1996]. A set of initial conditions and lower and lateral boundary conditions are required to complete SCM and CRM simulations. These initial and boundary conditions can be prescribed in ideal cases for theoretical studies or obtained from measurements in real cases for model results to be compared with observations. In real cases, the initial and boundary conditions need to be prescribed as accurately as possible.

The large-scale forcing fields (such as vertical velocity and advective tendencies) are part of the lateral boundary conditions describing the vertical and horizontal transports from adjacent regions. These fields cannot be directly observed, and simple estimations from the atmospheric state variables often contain large errors because of the errors in the derivative calculation. To obtain the large-scale forcing fields accurately, several objective methods have been developed based on the atmospheric radiosonde data [*Ooyama*, 1987; *Lin and Johnson*, 1996; *Zhang and Lin*, 1997; *Johnson et al*., 2015]. *Zhang and Lin* [1997] developed a constrained variational analysis algorithm to produce large-scale forcing data by using surface and the top of the atmosphere (TOA) measurements as constraints to adjust the large-scale state variables to conserve the column-integrated mass, moisture, heat, and momentum. This analysis method has been successfully used in the U.S. Department of Energy (DOE) Atmospheric Radiation Measurements (ARM) program for nearly 20 years for its large-scale forcing data development [*Zhang et al*., 2001; *Xie et al*., 2004, 2005, 2006; *Schumacher et al*., 2007, 2008; *Xie et al*., 2010a, 2014; *Tang et al*., 2016b] and various cloud modeling studies [*Ghan et al*., 2000; *Xie et al*., 2002; *Xu et al*., 2002; *Xie et al*., 2005; *Xu et al*., 2005; *Klein et al*., 2009; *Morrison et al*., 2009; *Fridlind et al*., 2012].

However, when the domain size is large for an atmospheric column, the lack of subcolumn scale spatial variability in current forcing data can be an issue to simulate cloud systems [*Ryan et al*., 2000; *Xie et al*., 2002, 2005; *Xu et al*., 2005]. The current large-scale forcing represents an average of a domain with the size of a couple hundred kilometers. When only part of the domain is affected by a convective system, the domain-mean large-scale forcing fields may not capture the subdomain scale features, which may cause problems in

SCM and CRM simulations [e.g., *Xie et al*., 2005; *Xu et al*., 2005]. As part of the ARM Global Energy and Water Cycle Exchanges Project Cloud System Studies (GCSS) case study, *Xie et al*. [2005] investigated a deep frontal case during 2–4 March 2000 at the ARM Southern Great Plains (SGP) site and found that errors in the SCM and CRM simulated clouds could be partially due to the application of the uniform large-scale forcing. Our study will revisit this deep frontal case focusing on how the spatial variability of the large-scale forcing fields affects SCM simulated precipitation and clouds.

With a continuously increasing number of measurements available at the ARM SGP site, recent studies have been exploring the ways of producing forcing data for domains smaller than the typical grid box size of a conventional atmospheric general circulation model (GCM). *Xie et al*. [2014] used the constrained variational analysis to derive the large-scale forcing data over different domain sizes (300 km, 150 km, and 75 km) for the Midlatitude Continental Convective Clouds Experiment field campaign and tested their sensitivity. They found that the timing and the vertical structure of upward motion are affected by the domain size. *Feng et al*. [2015] also derived forcing data over different domain sizes by using a multiscale data assimilation framework [*Li et al*., 2015] in the Weather Research and Forecasting model and investigated grid scale and subgrid scale components. They showed that the SCM simulations were sensitive to the grid scale and suggested that the subgrid scale dynamic component was important. Based on the constrained variational analysis algorithm from *Zhang and Lin* [1997] and *Zhang et al*. [2001], *Tang and Zhang* [2015] developed a three-dimensional constrained variational analysis (3DCVA) method and derived a gridded large-scale forcing data at 0.5° × 0.5° resolution for the March 2000 Intensive Operational Period (IOP) at SGP. *Tang and Zhang* [2015] showed that the derived forcing data could well describe the three-dimensional thermodynamic fields related to the 2–4 March deep frontal case as studied in *Xie et al*. [2005]. In the current study, our first objective is to use this gridded large-scale forcing data to further investigate its spatial variability and explore its impact on SCM simulated precipitation and clouds, in particular, the model errors identified in *Xie et al*. [2005]. Our second objective is to explore the potential use of the gridded forcing data to investigate the scale dependence of parameterization given the flexibility of constructing the gridded large-scale forcing data over different resolutions. Note that scale-aware parameterizations are being actively developed in the climate modeling community for use in climate models with a range of spatial resolutions. The gridded forcing data provides the needed forcing for testing scale-aware parameterizations in SCMs.

This paper is organized as follows. Section 2 describes the data used in this study and SCM setups. Section 3 illustrates the problem in SCM simulations with the domain-mean forcing. Section 4 investigates the impacts of using the gridded large-scale forcing in SCM simulations of a deep frontal system. Section 5 expands the work to a shallow frontal case and the whole IOP. Section 6 shows two examples where the gridded forcing data may be used to evaluate and understand model parameterizations. Section 7 presents a summary and discussion.

2. Data and Model Setup

2.1. Forcing and Evaluation Data

The gridded large-scale forcing data used in this study are obtained from an ensemble approach of 3DCVA described in *Tang et al*. [2016a], which has 90 members with different combinations of background fields, error covariance matrix, and constraint variables. In this study, we use the ensemble mean gridded forcing data derived from the same six different background fields as used in *Tang et al*. [2016a]. To reduce the computational cost, only one set of error covariance matrix (both horizontally and vertically correlated, see *Tang et al*. [2016a] for more information) and constraint variables (described below) is used. Detailed descriptions of the 3DCVA method and the ensemble approach can be found in *Tang and Zhang* [2015] and *Tang et al*. [2016a], respectively.

The constraint variables in the 3DCVA include data obtained from the ARM surface measurements, the 4 km resolution precipitation product from the Arkansas-Red Basin River Forecast Center (ABRFC), and the 0.5° × 0.5° resolution Geostationary Operational Environment Satellite (GOES) 8 product from NASA Langley Research Center. The ARM surface measurements at SGP include multiple instruments such as surface meteorology stations, Oklahoma and Kansas mesonet stations, solar and infrared observing systems, energy budget Bowen ratio stations, eddy correlation flux measurement systems, and microwave radiometer. These data are interpolated (averaged for precipitation) into 0.5° GOES grid boxes within a 5° × 4.5° domain

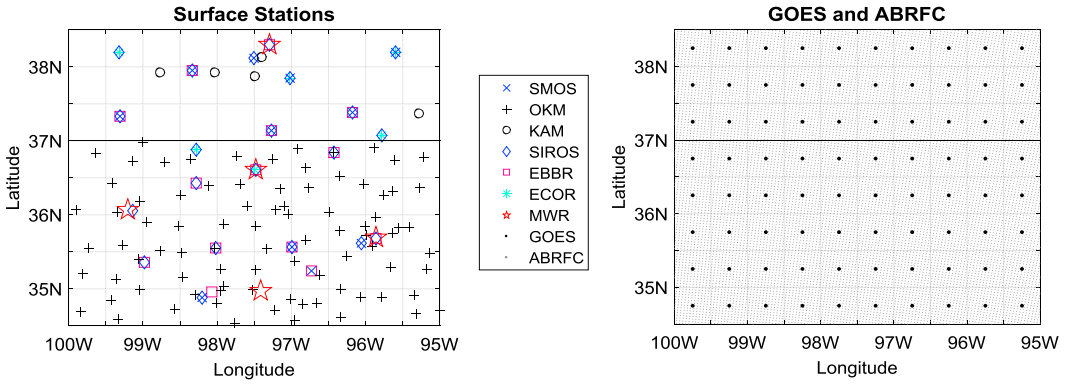

Figure 1. (left) Surface stations and (right) GOES TOA measurements and ABRFC gridded precipitation data. Different marks indicate different instruments (see text). The gray lines show 0.5° × 0.5° grids in 3DCVA which are the same as grids of GOES satellite products (black dots). The black line at 37°N indicates the boundary between Oklahoma (below) and Kansas (above) (revised from *Tang et al.* [2016a]).

(Figure 1). In total, there are 10 × 9 subcolumns within the 5° × 4.5° domain (referred to as analysis domain hereafter). The large-scale forcing fields are derived over each subcolumn as well as over the entire analysis domain.

The vertical profile of cloud frequency used in the model validation is obtained from the ARM Best Estimate [*Xie et al.*, 2010b] data set derived from the Active Remote-Sensed Cloud Locations (ARSCL) [*Atmospheric Radiation Measurement Climate Research Facility*, 1996] product. It provides a high-frequency cloud mask measured from a combination of the cloud radar, micropulse lidar, and ceilometer located at the SGP central facility. This product leverages each instrument's strengths: the cloud radar penetrates nonprecipitating and weakly precipitating thin clouds, the micropulse lidar is sensitive to thin clouds, and the ceilometer reliably detects cloud base. The high-frequency cloud mask is then averaged into 3 h cloud frequency to be consistent with the temporal resolution of the large-scale forcing data in this study. Note that a different averaging time window could be used to derive the cloud fraction over different sizes of domains for improving the comparison of SCM clouds with the observations. In practical, however, this is hard to achieve because wind speed changes with both time and height. This is the challenge to derive cloud fraction from the ARM single-point cloud observations. Since cloud patterns should not be changed with using different averaging time windows, the use of a 3 h temporal averaging for all the domains does not impact the qualitative analysis in this study.

2.2. SCM Setup

A SCM version of the Community Atmospheric Model version 5 (CAM5) [*Neale et al.*, 2012], known as SCAM5, is used to investigate the impact of the spatial variability of the forcing fields on simulated precipitation and clouds. The CAM5 physical parameterizations include a turbulent kinetic energy-based boundary layer scheme combined with a shallow convection scheme [*Bretherton and Park*, 2009; *Park and Bretherton*, 2009], a bulk two-moment cloud microphysics scheme for stratiform clouds [*Morrison and Gettelman*, 2008], the macrophysics scheme of *Park et al.* [2014], and the deep convection scheme of *Zhang and McFarlane* [1995]. Two sets of experiments are designed: The first one is running SCAM5 with the domain-mean forcing, representing traditional way of SCM simulation; the other experiment is running SCAM5 using the forcing in each subcolumn independently, then averaging them together. Although the SCAM5 simulations in different subcolumns are run independently, the forcing fields are mutually constrained among these subcolumns. The second set can be viewed as a "regional model" simulation in which the atmospheric dynamics is specified from observations. The differences between the two sets of experiments will show the nonlinear responses of SCM to the spatial variability of the large-scale forcing. In these experiments, no relaxation is applied so that the tendency terms only include model physical tendencies and large-scale tendencies from the forcing data. To allow clouds to have sufficient time to develop while the large-scale state has still not drifted too far away from the observations, SCAM5 was initiated every 3 h and run for 9 h during the March 2000 IOP (15 Z, 1 March, to 21 Z, 21 March), and only the hour 6 to 9 of each simulation are

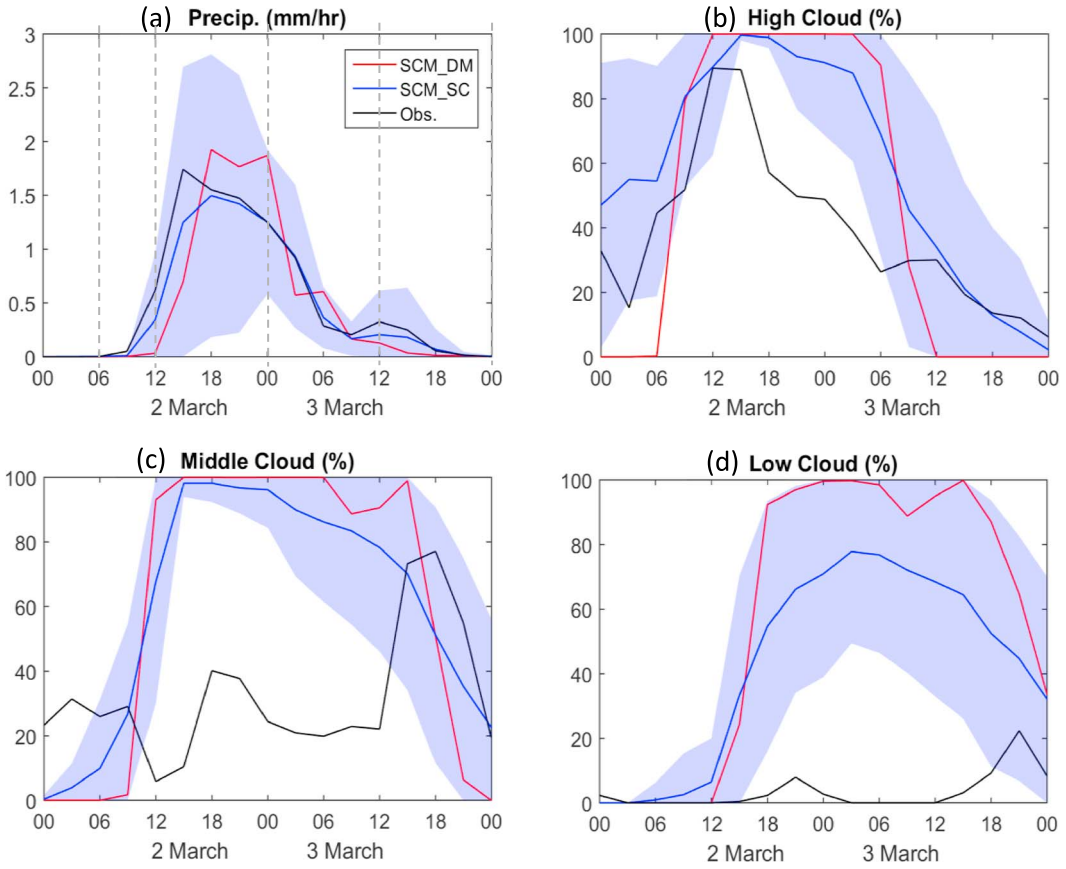

Figure 2. Time series of (a) surface precipitation, (b) high cloud, (c) middle cloud, and (d) low cloud. The black line represents the domain-mean observation (Obs.). The red line represents the SCAM5 simulation with domain-mean forcing (SCM_DM). The blue line and blue shade represent the mean of the SCAM5 simulations with subcolumn forcing (SCM_SC) and the spatial standard deviation, respectively. The gray dashed lines in Figure 2a show the timing of the five stages in Figures 3–5.

concatenated into the time series between 2 and 21 March. Surface latent and sensible heat fluxes are prescribed by observations so that the land and the atmosphere are not interactive. The March 2000 IOP includes several frontal systems propagating through the SGP site. This study mainly focuses on the deep frontal case that occurred from 2 to 4 March 2000. A shallow frontal cloud case from 16 to 19 March 2000 and the whole IOP are also analyzed. Details of the synoptic conditions and the three-dimensional structures of these two cases can be seen in *Xie et al*. [2005], *Xu et al*. [2005], and *Tang and Zhang* [2015].

3. Problems of Using the Domain-Mean Forcing in SCAM5 Simulations

In *Xie et al*. [2005], some SCM errors are attributed to the use of domain-mean forcing. We start our analysis by revisiting the same case. Figure 2 shows the comparison of the simulated surface precipitation and clouds using the domain-mean forcing (red line) and the domain-mean observations (black line) for the 2–4 March deep frontal case. The dashed lines in Figure 2a indicate the five evolution stages of the frontal system analyzed in this study. Figure 3 shows the spatial pattern of the observed precipitation and clouds during the five evolution stages. Since middle and low clouds in satellite measurements may be missed due to overlapping of clouds in vertical, we only focus on high clouds in Figure 3. No precipitation is observed at stage 1 since the front had not come into the domain, but high clouds ahead of the front had already moved in and occupied the western part of the domain. At stage 2, along with the propagation of the front into the analysis domain, precipitation occurred in the western part of the analysis domain, with high clouds occupying most of the domain. At stage 3, the front moved northeastward, along with the precipitation and high clouds. At stage 4, the entire domain is under the influence of the back of the comma head with some

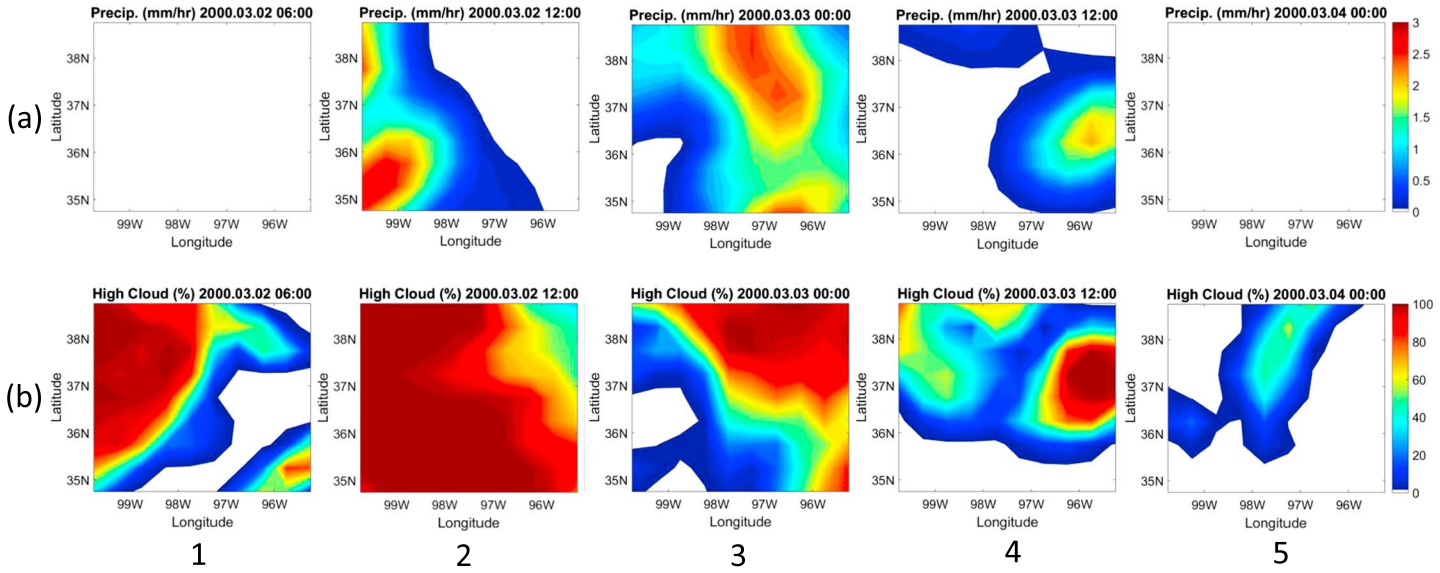

Figure 3. Horizontal distribution of observed (a) precipitation and (b) high clouds for the five stages (indicated in Figure 2a) of the deep frontal case.

associated precipitation and high clouds. The whole system moved out of the domain at stage 5 along with some high clouds and no precipitation.

Given that the large-scale forcing is constrained by the observed surface precipitation, it is not surprising to see that the simulated precipitation generally agrees with the observation (Figure 2a). However, two model errors are noted. One is the delay of the precipitation onset around 12 Z, 2 March; the other is the lack of a secondary peak around 12 Z, 3 March. These errors can also be seen in other SCMs and are postulated to be due to the lack of spatial variability in the large-scale forcing data [*Xie et al*., 2005].

Figures 2b–2d compare the simulated high, middle, and low cloud fractions with the observations. The thresholds of vertical levels between high and middle, middle, and low clouds in CAM5 were modified to be consistent with the thresholds used in the satellite measurements (6 km and 2 km, respectively). The model with domain-mean forcing overestimates high clouds during the passage of the frontal system and underestimates high clouds before and after it. Generally, it shows an "all-or-nothing" feature (e.g., jumping from 0% to 100% around 06 Z, 2 March, and from 100% to 0% around 12 Z, 3 March), which is different from the slow transition seen in the observation. The observed middle and low clouds are most likely underestimated due to the overlapping of clouds. The simulated middle and low clouds using domain-mean forcing also show an all-or-nothing feature, similar to the high clouds. This difference between simulated and observed clouds can be due to several reasons besides the limitation of observations, including the lack of hydrometeor advection in the current forcing data, potential forcing errors, and deficiencies in the physical parameterization. The lack of subdomain spatial variability with the use of the domain-mean forcing may also contribute to the model errors. In the next section, we will investigate the spatial variability of the large-scale forcing and explore the impact of considering the spatial variability in SCM simulations.

4. Impact of the Subcolumn Forcing on SCAM5 Simulations

The large spatial variability of the observed precipitation and high clouds shown in Figure 3 indicates that the large-scale forcing fields may also have large spatial variability. Figure 4 shows the vertical profiles of vertical velocity (omega), total advection of dry static energy s (Tadvs), and total advection of specific humidity q (Tadvq) profiles at the five stages. The gray lines indicate profiles in each subcolumn. The black solid and dashed lines indicate the domain-mean profiles and the mean of the subcolumn profiles, respectively. For Tadvs and Tadvq, the black solid lines and black dashed lines are not exactly overlapped. This is because the domain-mean large-scale advection ($\overline{V}\cdot\nabla\overline{s}$ or $\overline{V}\cdot\nabla\overline{q}$) is not the same as the mean of subcolumn advection ($\overline{V\cdot\nabla s}$ or $\overline{V\cdot\nabla q}$). Their difference represents subgrid advection ($\overline{V'\cdot\nabla s'}$ or $\overline{V'\cdot\nabla q'}$).

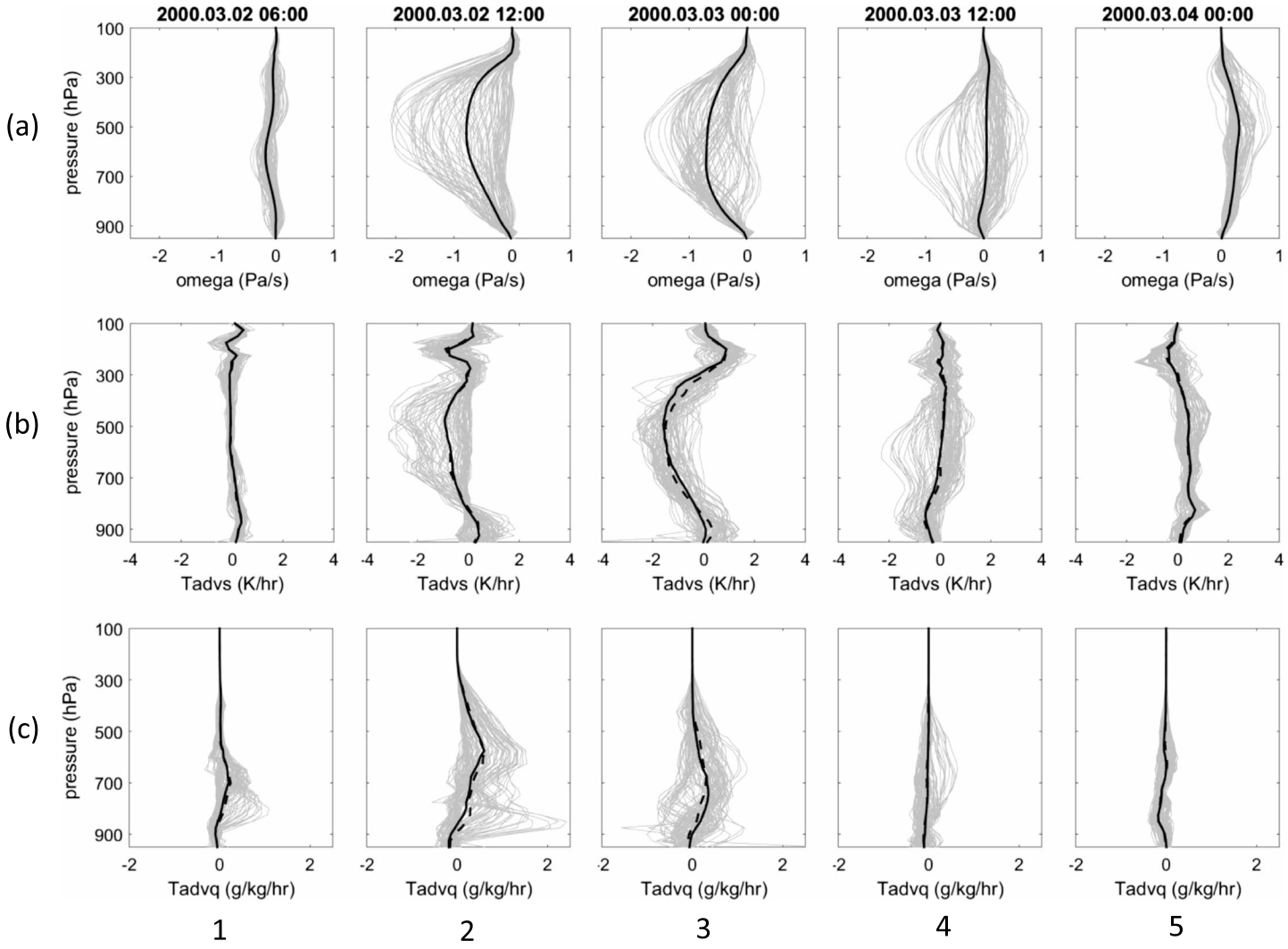

Figure 4. (a) Large-scale vertical velocity (omega), (b) total advection of dry static energy (Tadvs), and (c) total advection of moisture (Tadvq) for the five stages of the deep frontal case. The black solid line is the domain-mean profile. The black dashed line is the mean of all subcolumn profiles (gray lines). The difference between the domain-mean and the mean of subcolumn Tadvs and Tadvq is due to subgrid advections.

At stage 1, the large-scale forcing is weak and the spatial variabilities are relatively small. At stages 2 and 3, there are upward motions throughout the troposphere, with strong advection of energy and moisture. The spatial variabilities are also large. At stage 4 when there is a wrap-in system, there is upward motion in a few subcolumns and downward motion in many others; thus, the domain-mean large-scale forcing is very weak but the spatial variability is still large. At stage 5 after the front moved out of the domain, the domain-mean forcing is weak and the spatial variability is small again, similar to that before the front moved in the domain.

The spatial variability of the large-scale forcing can qualitatively explain the differences between the simulated and observed precipitation in Figure 2a. When the forcing data have small spatial variability (stages 1 and 5), the domain-mean large-scale forcing data work well, with simulated precipitation close to the observation. When only a small part of the domain has strong forcing and a large part has weak forcing (stages 2 and 4), the domain-mean forcing may not be strong enough to produce as much precipitation as observed. When most of the domain has strong forcing but a small part has weak forcing (stage 3), the domain-mean forcing may be strong enough for SCAM5 to produce more precipitation than the observation.

The gridded large-scale forcing data are applied by running SCAM5 over each subcolumn of the analysis domain, as a small regional model. The spatial distributions of simulated precipitation at the five stages of

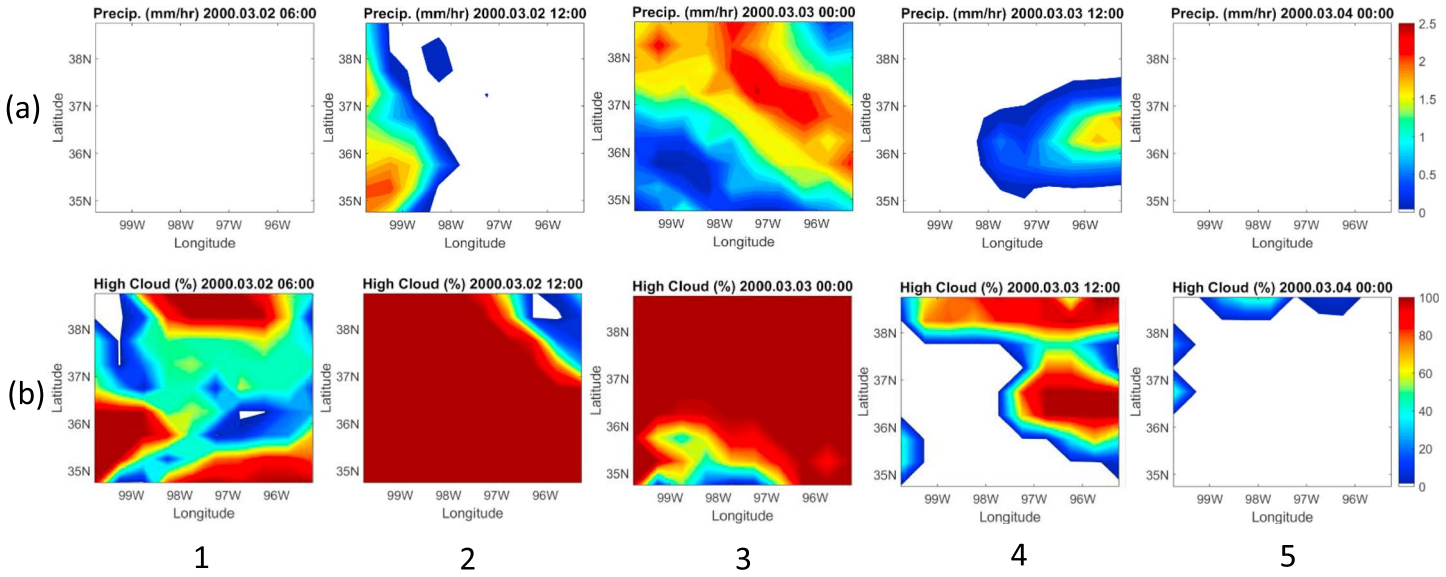

Figure 5. Horizontal distribution of SCAM5 simulated (a) surface precipitation and (b) high clouds for the five stages of the deep frontal case. SCAM5 are driven in each subcolumn of the SGP domain.

the deep frontal case are shown in Figure 5a. Compared to Figure 3a, the precipitation patterns agree with the observation very well. We also generated the domain-mean precipitation by averaging the simulated precipitation using forcing data in each subcolumn and calculated the spatial standard deviation. These are shown as the blue line and shading in Figure 2a. It is seen that the mean SCM simulations with subcolumn forcing considerably reduced the delay in the precipitation onset. It also produced the secondary peak around 12 Z, 3 March. Note that the large-scale forcing in both simulations used the observed precipitation as constraints. The difference between the two simulations is therefore primarily due to the impact of the nonlinear response of precipitation to subcolumn scale forcing.

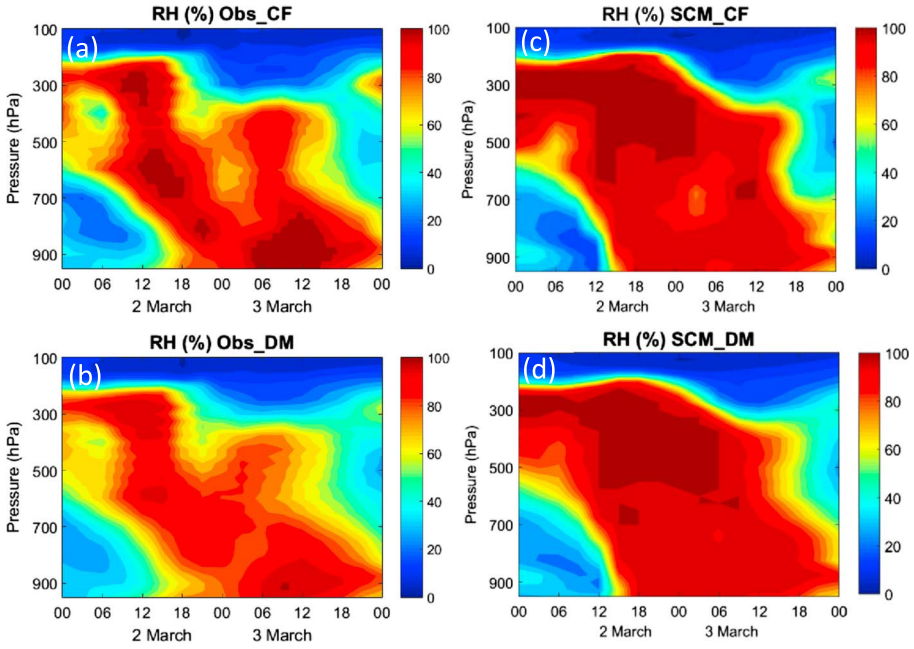

Figure 6. Time-pressure cross section of (a and b) observed and (c and d) SCAM5 simulated relative humidity. Figures 6a and 6c are in the subcolumn closest to the central facility (CF). Figures 6b and 6d are averaged in the analysis domain (DM).

Table 1. Comparison of Precipitation and High Clouds at the Five Stages of the Front Case[a]

Stage		1	2	3	4	5
Precip. (mm h^{-1})	SCM_SC	0.00 ± 0.00	0.34 ± 0.62	1.25 ± 0.67	0.21 ± 0.41	0.00 ± 0.00
	SCM_DM	0.00	0.03	1.87	0.13	0.00
	Obs.	0.01	0.69	1.24	0.32	0.00
High clouds (%)	SCM_SC	54.5 ± 35.7	89.8 ± 27.3	91.2 ± 22.6	33.9 ± 41.0	2.2 ± 8.9
	SCM_DM	0.3	100	100	0.0	0.0
	Obs.	41.8	84.7	47.7	28.7	6.2

[a]SCM_SC represents domain-mean SCAM5 simulations with forcing data in each subcolumn. SCM_DM represents SCAM5 simulation with domain-mean forcing data. Obs. represents domain-mean observations. The spatial standard deviations of SCM simulations with subcolumn forcing are also shown.

The high clouds simulated by the SCM with the subcolumn forcing at the five stages of the frontal case are shown in Figure 5b. It clearly captured a certain level of subcolumn scale variability of high clouds during the passage of the front (Figure 3b). As a result, the transition of high clouds is better simulated (Figure 2b), even though there is an overall overestimation of high cloud amount throughout the period. It is known that the overestimation of high clouds is a typical model error in CAM5 [e.g., *Tang et al*., 2016a], and cloud formation in CAM5 is largely controlled by relative humidity. During the passage of the front, the relative humidity in the upper troposphere is generally overestimated (Figure 6). Thus, more high clouds are simulated. The cause of the overestimation of relative humidity is subject to future investigation. The middle and high clouds simulated with the subcolumn forcing also show more transition than simulated with the domain-mean forcing (Figures 2c and 2d), but the comparison with the observations is difficult due to the overlapping limitation.

Table 1 compares the domain-mean precipitation and high clouds from the SCAM5 simulations using subcolumn forcing (SCM_SC) and domain-mean forcing (SCM_DM), along with domain-mean observations (Obs.) at the five stages. Overall, the mean results in each of the five stages from using subcolumn forcing agree better with observations than from using the domain-mean forcing.

5. The Shallow Cloud Case and the Whole IOP

In this section, we extend our analysis to a shallow cloud case, as well as the whole March 2000 IOP, to examine how the gridded forcing data impact SCM simulations of different synoptic systems.

5.1. The Shallow Cloud Case

We applied similar analysis for the shallow frontal case from 16 to 19 March that was studied in *Xu et al*. [2005]. The observed cloud frequency from the ARSCL cloud product is shown in Figure 7. This case includes a period between 03 Z, 17 March, and 06 Z, 18 March, that is dominated by shallow frontal clouds with dry and nearly clear sky in the middle and upper troposphere. Details about the synoptic conditions of this system can be found in *Xu et al*. [2005].

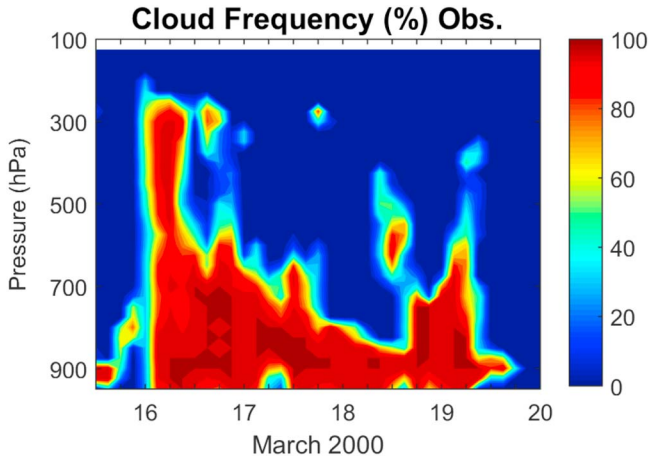

Figure 7. Observed cloud frequency (%) for the shallow frontal case from ARSCL product.

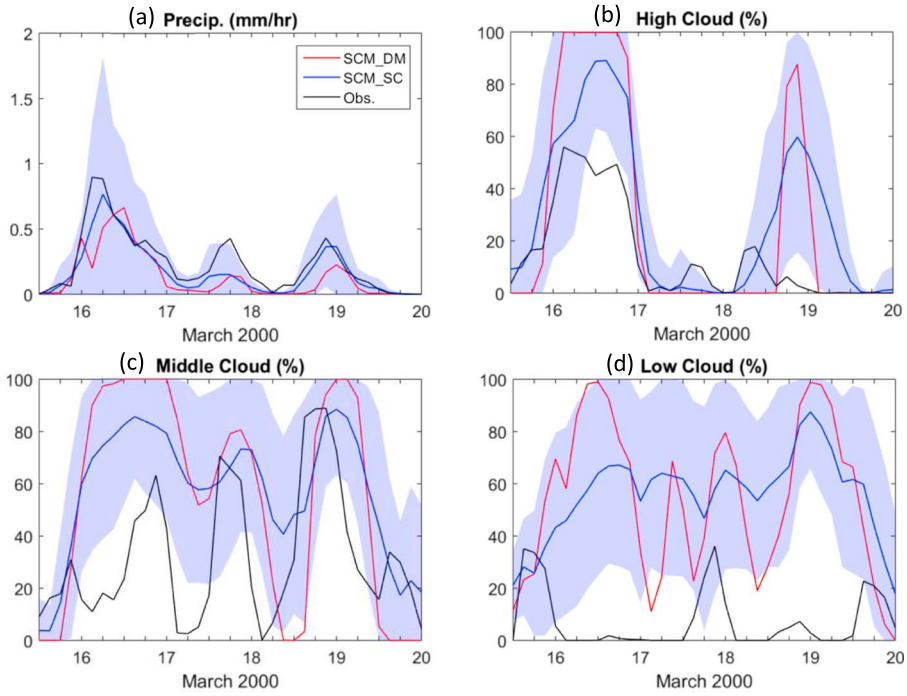

Figure 8. Similar as Figure 2 but for the 16–19 March shallow frontal case.

Figure 8 shows the domain-averaged precipitation (Figure 8a) and high, middle, and low (Figures 8b–8d) clouds from SCAM5 with domain-mean forcing (SCM_DM), with subcolumn forcing (SCM_SC), and from observations (Obs.). A late onset of precipitation and little cloud transition are also seen in the SCM_DM run, similar to the deep frontal case. By considering the subcolumn scale variability, SCM_SC captures the timing of precipitation and transition of clouds better than SCM_DM for this shallow cloud case.

5.2. The Whole IOP

Figure 9 shows the domain-averaged precipitation, clouds, liquid water path (LWP), and radiative fluxes from SCM_DM, SCM_SC, and Obs. for the whole IOP. The precipitation onset and cloud transition are improved in SCM_SC for most of the time. LWP and radiative fluxes in SCM_SC are also closer to the Obs. than SCM_DM. To quantitatively evaluate the results, we further calculated the root-mean-square errors (RMSE) of these variables in SCAM5 simulations relative to observational estimates for the whole IOP period from 2 to 21 March 2000 (Table 2). For all of the variables, SCM_SC has smaller RMSE than SCM_DM. The results of the additional case study and the overall analysis give us more confidence that our previous conclusions are robust for different synoptic systems at the SGP site.

6. Applications of Gridded Large-Scale Forcing Data

In this section, we will briefly discuss two examples of how gridded large-scale forcing data may be used in model evaluation and development.

6.1. Comparison With Point Measurements

Xie et al. [2005] showed in the ARM-GCSS case study that the majority of SCMs and CRMs failed to simulate the time transition of the middle and low clouds during the frontal passage when the model simulations are compared with cloud radar measurements. They speculated that the cause of this deficiency is partly due to the mismatch of the scale between the domain-averaged model representation and the vertically pointed radar data. The spatial distribution of the subcolumn scale variability of the large-scale forcing data allows us to revisit this problem.

Figure 10 compares the pressure-time cross section of observed and simulated clouds in the 2–4 March frontal case. Figure 10a is the observations from the ARSCL cloud product. Figure 10b is the simulation

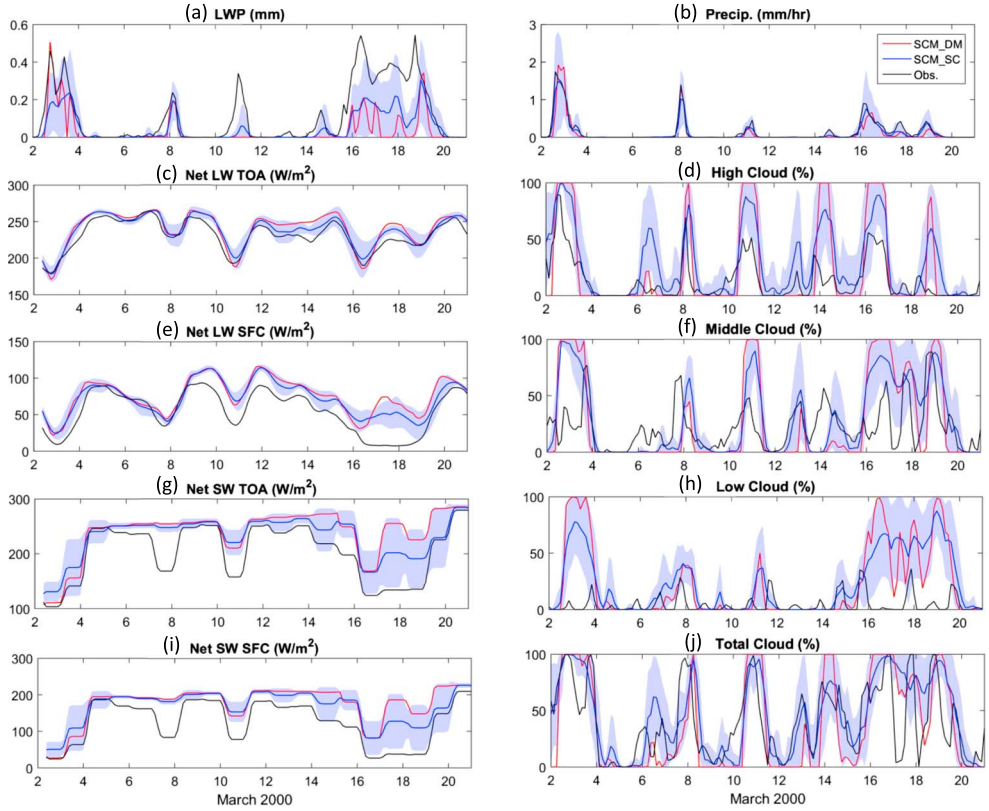

Figure 9. Time series of (a) liquid water path (LWP), (b) surface precipitation, (c) net longwave flux at TOA, (d) high cloud, (e) net longwave fluxes at surface, (f) middle cloud, (g) net shortwave fluxes at TOA, (h) low cloud, (i) net shortwave fluxes at surface, and (j) total cloud fraction for the whole March 2000 IOP. The lines are similar as Figure 2. The 24 h running average is applied on longwave and shortwave fluxes.

using the subcolumn forcing closest to the central facility (SCM_CF), while Figure 10c is the simulation using the domain-mean forcing (SCM_DM). The difference in the forcing between the two simulations here is due to the different scales. It is seen that the model with the "CF" forcing was able to capture the midlevel cloud break during 00 to 06 Z, 3 March. This feature is not clearly shown in the model with the domain-mean forcing. The difference of simulated clouds is consistent with the difference of relative humidity (RH) shown in Figure 6. The subcolumn RH closest to the central facility shows a dry period at 800–500 hPa during 00 to 06 Z, 3 March, corresponding to the cloud break. The domain-mean RH does not capture this dry period. Instead, it dries out too early in the middle atmosphere. This is probably because the scale of the cloud break and wrap-in cloud system is smaller than the size of the analysis domain, so that the domain-mean fields are not able to capture the large-scale features, which causes a bias in the cloud simulations. While it is known that model results are different when different scales of forcing are used, this illustration confirms the speculation in *Xie et al.* [2005] that a significant part of the common model error in that GCSS study can indeed be attributed to the mismatch of the scales between forcing and the

Table 2. RMSE of Domain-Mean Precipitation (PREC, mm h^{-1}), Liquid Water Path (LWP, cm), Total Cloud (CLDT, %), High Cloud (CLDH, %), Middle Cloud (CLDM, %), Low Cloud (CLDL, %), Net Longwave Fluxes at TOA (LWT, W m^{-2}), Net Shortwave Fluxes at TOA (SWT, W m^{-2}), Net Longwave Fluxes at Surface (LWS, W m^{-2}), and Net Shortwave Fluxes at Surface (SWS, W m^{-2}) for the Whole March 2000 IOP (2–20 March)[a]

	PREC	LWP	CLDT	CLDH	CLDM	CLDL	LWT	SWT	LWS	SWS
SCM_DM	0.155	0.152	32.2	28.9	36.7	36.8	21.6	50.1	34.6	64.5
SCM_SC	0.084	0.123	27.4	24.4	30.3	32.0	17.8	37.7	29.1	50.6

[a]SCM_DM represents SCAM5 simulation with domain-mean forcing data, and SCM_SC represents domain-mean SCAM5 simulations with forcing data in each subcolumn.

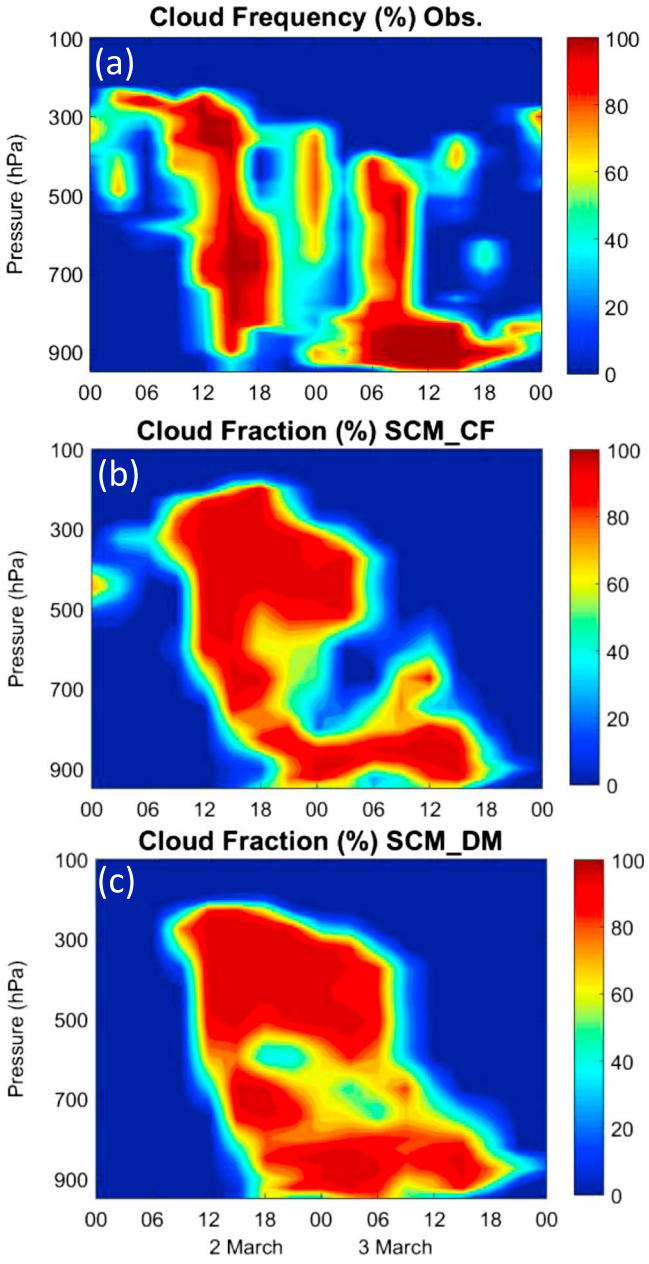

Figure 10. Time-pressure cross section of cloud frequency (fraction) from (a) ARSCL observation at SGP central facility, (b) SCAM5 simulation using the forcing of the subcolumn closest to the central facility (SCM_CF), and (c) SCAM5 simulation using the domain-mean forcing (SCM_DM).

observed clouds. It also shows that the gridded forcing data can be configured to the same scale as the cloud observation so that scale-aware parameterizations can be studied as described below.

6.2. Investigating Scale-Aware Parameterizations

There is an increasing need to develop scare-aware parameterizations in climate models with a range of spatial resolutions. The gridded forcing data can be used to evaluate scale-aware parameterizations in several ways. For example, by using forcing data at different scales, one can use a simulation performance metric and examine how it varies with the scale when the parameterization is forced by data and evaluated against observations at the same scale. If a parameterization was designed only for a particular scale but ought to be scale dependent, one can expect to see that the performance metric is likely better at this scale than at other scales. The evaluation results can provide insight on how the parameterization should be modified. One can also compare the scale dependences of performance metrics from two parameterizations to evaluate whether a parameterization is more scale-aware than the other scheme. The stronger is the dependence of the performance metrics on the imposed scales, the less is the scale awareness of a parameterization. The unique value of the gridded forcing data is the significantly increased data samples and flexibility to enable configurations of forcing and observational data at the same scales for such studies.

As a demonstration, we made the RH threshold for high cloud fraction (rhminh) in the CAM5 parameterization [*Neale et al.*, 2012] "scale-aware" and used the forcing data in different spatial resolutions to test the SCAM5. The default setting of SCAM5 is rhminh = 0.80. In the scale-aware experiment, we set rhminh = 0.65 for the 10 × 9 subcolumn domain and rhminh = 0.90 for the 1 × 1 subcolumn. These values are chosen based on the assumption that larger domain will include more subgrid inhomogeneity so that clouds can form under a lower environmental RH. The RH threshold for an intermediate domain is set from a near-linear relationship between the 10 × 9 domain and the 1 × 1 subcolumn (e.g., for the 4 × 3 subcolumn domain, rhminh is set as 0.82). The simulated cloud fraction for the 2–4 March frontal case is determined primarily by stratiform clouds so that the threshold of RH is an important parameter for the cloud fraction. Convective cloud fraction is negligible (not shown).

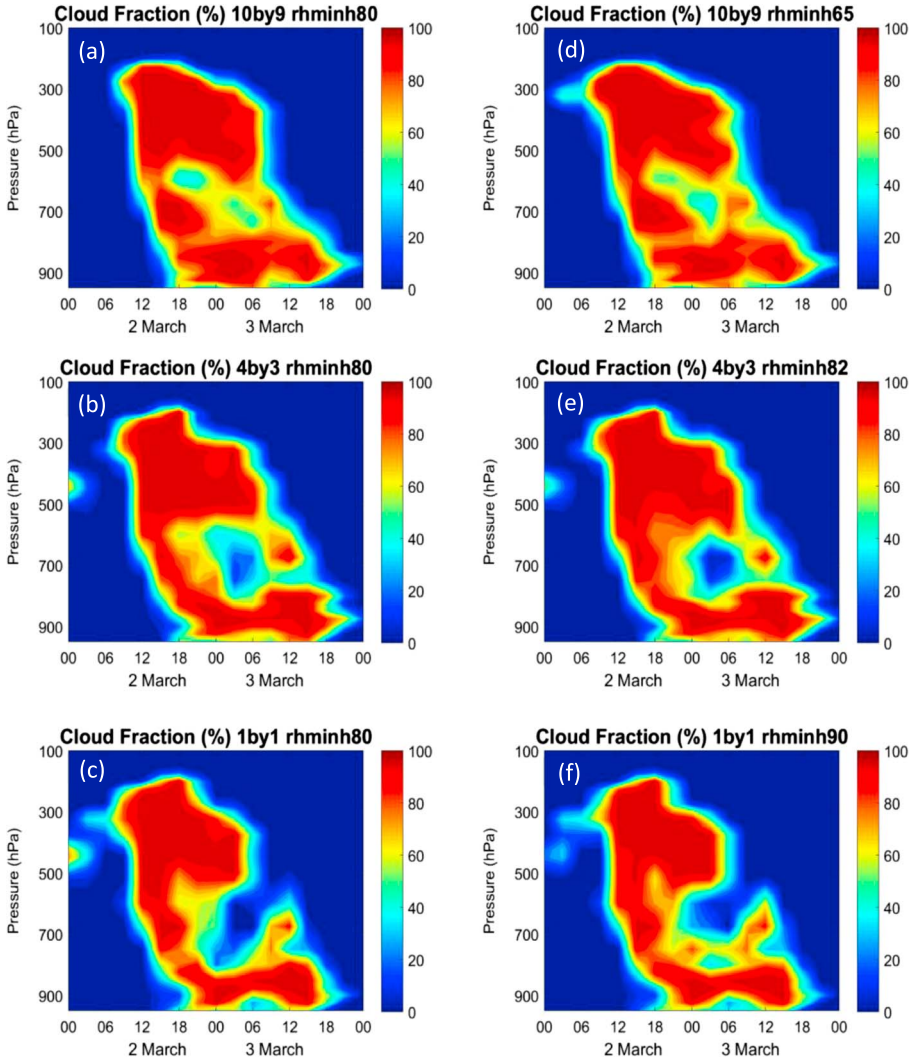

Figure 11. Time-pressure cross section of simulated cloud fraction in different model configurations: (a–c) using fixed RH threshold rhminh = 80% and (d–f) using scale-aware RH threshold with changing rhminh with scale. Figures 11a and 11d are run with the 10 × 9 grids-mean forcing. Figures 11b and 11e are run with the 4 × 3 grids-mean forcing centered at the central facility. Figures 11c and 11f are run with the forcing of 1 × 1 grid closest to the central facility.

Figure 11 shows the SCAM5 simulated clouds driven by the large-scale forcing data averaged in the 10 × 9 subcolumn domain (Figures 11a and 11d), 4 × 3 subcolumn domain (Figures 11b and 11e), and 1 × 1 subcolumn (Figures 11c and 11f), centered at the central facility. Figures 11a–11c use the default fixed setting of rhminh = 0.80; Figures 11d–11f use a scale-aware setting of rhminh described in the previous paragraph. The differences in cloud fraction across scales are due to the forcing at different resolutions, while the differences between fixed and scale-dependent rhminh show the impact of the scale-aware parameterization. Since we do not have the time-pressure cross section of clouds at different resolutions from observation to compare the metric, we calculated the RMSE of simulated high clouds comparing to the satellite observations in the corresponding domain sizes (Table 3). The differences between simulations with "fixed" and scale-aware parameters are relatively minor, but using the scale-aware parameterization does show smaller RMSE than the fixed parameterization. For the 10 × 9 domain, rhminh is lower in the scale-aware parameterization; thus, high clouds appear earlier in Figure 11d than Figure 11a. This is more consistent with the observations in Figure 2b.

This experiment is very simple and does not hint which value should be used for the RH threshold. Our goal is just to demonstrate that the gridded large-scale forcing data can be used toward the direction of testing

Table 3. RMSE of High Cloud (%) for the SCAM5 Simulations in Different Domain During the Period of 2–4 March[a]

	10 × 9	4 × 3	1 × 1
Fixed	34.35	35.98	35.04
Scale-aware	32.78	34.86	33.31

[a]Fixed represents simulations using fixed parameterizations (rhminh = 0.80); scale-aware represents simulations using scale-dependent parameterizations (rhminh = 0.65 for 10 × 9 domain, rhminh = 0.82 for 4 × 3 domain, and rhminh = 0.90 for 1 × 1 domain).

scale-aware parameterizations. A test of real scale-aware parameterizations will be subject to future study and is beyond the scope of this paper.

7. Summary and Discussion

Although domain-mean large-scale forcing data have been successfully used in driving SCM/CRM for about two decades, studies have shown that under some circumstances such as for midlatitude frontal systems, the lack of spatial variability may cause problems in model simulations. This study revisits the cases studied in *Xie et al*. [2005] and investigates the impact of the spatial variability in the forcing fields by using a gridded large-scale forcing data set from a 3-D constrained variational analysis method derived by *Tang and Zhang* [2015] and *Tang et al*. [2016a]. We have shown that SCAM5 with the domain-mean forcing has difficulty to capture the convective systems when they are partly located in the domain or only occupy a small part of the domain. This model problem is partly related to the lack of spatial variability in the forcing fields.

The gridded large-scale forcing data describe the spatial variability of the large-scale environment. When SCAM5 is run in each subcolumn of the domain, the simulation in a frontal case reduces the delay of the precipitation onset and produces the secondary peak which is missing in the simulation with domain-mean forcing. It also captures the transition feature of the domain-mean high clouds, although the overall cloud fraction is still overestimated. The simulations for a case of shallow frontal clouds and the whole March 2000 IOP are also shown with improvement when compared with observation.

We wish to point out that this study was conducted during the period of spring time in the midlatitude continent for frontal systems with large spatial variability. For a relatively homogeneous large-scale condition such as in the tropical region, domain-mean forcing data may be sufficient to represent the large-scale environment. Further analysis shows that during the nonprecipitation period of the March 2000 IOP (typically with smaller spatial variability), the RMSE differences between simulations with domain-mean forcing and with subcolumn forcing are found to be small.

The gridded large-scale forcing data have been newly developed, and we are exploring ways of its applications. Its most unique value is the many samples of the large-scale forcing across different spatial resolutions, which can be used to describe the spatial variability of the forcing and to conduct ensemble simulations of SCM. By configuring the gridded large-scale forcing data into different resolutions, we can investigate the scale mismatch between model simulations with point measurements and investigate the scale dependence of parameterizations as we demonstrated in this study. Some other potential uses of the subcolumn scale forcing data in driving, evaluating, and improving cloud/climate models are discussed below.

1. We can obtain a probability distribution function (PDF) of the large-scale forcing based on its spatial variability and implement it in SCMs to avoid running it in many columns. The PDF of the forcing can be used to test the SCM sensitivity and to investigate the nonlinear response of model physics to dynamics. It is expected that the PDF would be different for different kinds of systems (e.g., calm, clear days; summer convections; midlatitude frontal systems; and tropical MCSs); thus, the model response would also be different.
2. Although the gridded large-scale forcing data are intended to describe subcolumn variability within one model grid, the 0.5° subcolumn resolution is also close to the resolution of some current GCMs or regional models. Therefore, the gridded forcing data can also be used to evaluate the three-dimensional structure of model results in a small domain.

Finally, it would be interesting to study the spatial variabilities for different synoptic systems over different regions. To derive reliable gridded large-scale forcing data, however, high-density surface observations are

needed to obtain reliable 2-D constraints. It is hoped that the availability of high temporal and spatial resolution data such as the precipitation product from the bias-corrected National Mosaic and Multisensor Quantitative Precipitation Estimate constructed from the Next-Generation Radars [*Zhang et al.*, 2011] will make the characterization of these spatial variabilities possible.

Acknowledgments
This research is supported by the Biological and Environmental Research Division in the Office of Sciences of the U.S. Department of Energy (DOE). Work at LLNL was supported by the DOE Atmospheric Radiation Measurement (ARM) program and performed under the auspices of the U. S. Department of Energy by Lawrence Livermore National Laboratory under contract DE-AC52-07NA27344. Work at Stony Brook was supported by the Office of Science of the U. S. Department of Energy and by the National Science Foundation. All the data sets used in this study, including the ARM surface measurements, satellite data and ABRFC precipitation data, are available for download at the ARM Archive (http://www.archive.arm.gov/discovery/).

References

Atmospheric Radiation Measurement Climate Research Facility (1996), Atmospheric Radiation Measurement (ARM) Climate Research Facility, updated hourly. Active Remotely-Sensed Cloud Locations (ARSCL1CLOTH). 2000-03-01 to 2000-03-21, Southern Great Plains (SGP) Central Facility, Lamont, OK (C1). Compiled by K. Johnson and M. Jensen. Atmospheric Radiation Measurement (ARM) Climate Research Facility Data Archive: Oak Ridge, Tennessee, USA. Data set accessed 2016-07-23 at doi:10.5439/1027282.

Bretherton, C. S., and S. Park (2009), A new moist turbulence parameterization in the community atmosphere model, *J. Clim.*, *22*(12), 3422–3448, doi:10.1175/2008JCLI2556.1.

Feng, S., Z. Li, Y. Liu, W. Lin, M. Zhang, T. Toto, A. M. Vogelmann, and S. Endo (2015), Development of fine-resolution analyses and expanded large-scale forcing properties: 2. Scale awareness and application to single-column model experiments, *J. Geophys. Res. Atmos.*, *120*, 667–677, doi:10.1002/2014JD022254.

Fridlind, A. M., et al. (2012), A comparison of TWP-ICE observational data with cloud-resolving model results, *J. Geophys. Res.*, *117*, D05204, doi:10.1029/2011JD016595.

Ghan, S., et al. (2000), A comparison of single column model simulations of summertime midlatitude continental convection, *J. Geophys. Res.*, *105*(D2), 2091–2124, doi:10.1029/1999JD900971.

Johnson, R. H., P. E. Ciesielski, J. H. Ruppert, and M. Katsumata (2015), Sounding-based thermodynamic budgets for DYNAMO, *J. Atmos. Sci.*, *72*(2), 598–622, doi:10.1175/JAS-D-14-0202.1.

Klein, S. A., et al. (2009), Intercomparison of model simulations of mixed-phase clouds observed during the ARM Mixed-Phase Arctic Cloud Experiment. I: Single-layer cloud, *Q. J. R. Meteorol. Soc.*, *135*(641), 979–1002, doi:10.1002/qj.416.

Li, Z., S. Feng, Y. Liu, W. Lin, M. Zhang, T. Toto, A. M. Vogelmann, and S. Endo (2015), Development of fine-resolution analyses and expanded large-scale forcing properties: 1. Methodology and evaluation, *J. Geophys. Res. Atmos.*, *120*, 654–666, doi:10.1002/2014JD022245.

Lin, X., and R. H. Johnson (1996), Heating, moistening, and rainfall over the western Pacific warm pool during TOGA COARE, *J. Atmos. Sci.*, *53*(22), 3367–3383, doi:10.1175/1520-0469(1996)053<3367:HMAROT>2.0.CO;2.

Morrison, H., and A. Gettelman (2008), A new two-moment bulk stratiform cloud microphysics scheme in the Community Atmosphere Model, Version 3 (CAM3). Part I: Description and numerical tests, *J. Clim.*, *21*(15), 3642–3659, doi:10.1175/2008JCLI2105.1.

Morrison, H., et al. (2009), Intercomparison of model simulations of mixed-phase clouds observed during the ARM Mixed-Phase Arctic Cloud Experiment. II: Multilayer cloud, *Q. J. R. Meteorol. Soc.*, *135*(641), 1003–1019, doi:10.1002/qj.415.

Neale, R. B., et al. (2012), Description of the NCAR Community Atmosphere Model (CAM 5.0), 274 pp., NCAR Technical Note, *NCARTN-4861STR*. [Available at http://www.cesm.ucar.edu/models/cesm1.2/cam/docs/description/cam5_desc.pdf.]

Ooyama, K. V. (1987), Scale-controlled objective analysis, *Mon. Weather Rev.*, *115*(10), 2479–2506, doi:10.1175/1520-0493(1987)115<2479:SCOA>2.0.CO;2.

Park, S., and C. S. Bretherton (2009), The University of Washington shallow convection and moist turbulence schemes and their impact on climate simulations with the Community Atmosphere Model, *J. Clim.*, *22*(12), 3449–3469, doi:10.1175/2008JCLI2557.1.

Park, S., C. S. Bretherton, and P. J. Rasch (2014), Integrating cloud processes in the Community Atmosphere Model, Version 5, *J. Clim.*, *27*(18), 6821–6856, doi:10.1175/jcli-d-14-00087.1.

Randall, D. A., K.-M. Xu, R. J. C. Somerville, and S. Iacobellis (1996), Single-column models and cloud ensemble models as links between observations and climate models, *J. Clim.*, *9*(8), 1683–1697, doi:10.1175/1520-0442(1996)009<1683:SCMACE>2.0.CO;2.

Ryan, B. F., et al. (2000), Simulations of a cold front by cloud-resolving, limited-area, and large-scale models, and a model evaluation using in situ and satellite observations, *Mon. Weather Rev.*, *128*(9), 3218–3235, doi:10.1175/1520-0493(2000)128<3218:SOACFB>2.0.CO;2.

Schumacher, C., M. H. Zhang, and P. E. Ciesielski (2007), Heating structures of the TRMM field campaigns, *J. Atmos. Sci.*, *64*(7), 2593–2610, doi:10.1175/JAS3938.1.

Schumacher, C., P. E. Ciesielski, and M. H. Zhang (2008), Tropical cloud heating profiles: Analysis from KWAJEX, *Mon. Weather Rev.*, *136*(11), 4289–4300, doi:10.1175/2008MWR2275.1.

Tang, S., and M. Zhang (2015), Three-dimensional constrained variational analysis: Approach and application to analysis of atmospheric diabatic heating and derivative fields during an ARM SGP intensive observational period, *J. Geophys. Res. Atmos.*, *120*, 7283–7299, doi:10.1002/2015JD023621.

Tang, S., M. Zhang, and S. Xie (2016a), An ensemble constrained variational analysis of atmospheric forcing data and its application to evaluate clouds in CAM5, *J. Geophys. Res. Atmos.*, *121*, 33–48, doi:10.1002/2015JD024167.

Tang, S., et al. (2016b), Large-scale vertical velocity, diabatic heating and drying profiles associated with seasonal and diurnal variations of convective systems observed in the GoAmazon2014/5 experiment, *Atmos. Chem. Phys.*, *16*(22), 14,249–14,264, doi:10.5194/acp-16-14249-2016.

Xie, S., et al. (2002), Intercomparison and evaluation of cumulus parametrizations under summertime midlatitude continental conditions, *Q. J. R. Meteorol. Soc.*, *128*(582), 1095–1135, doi:10.1256/003590002320373229.

Xie, S., et al. (2005), Simulations of midlatitude frontal clouds by single-column and cloud-resolving models during the Atmospheric Radiation Measurement March 2000 cloud intensive operational period, *J. Geophys. Res.*, *110*, D15S03, doi:10.1029/2004JD005119.

Xie, S., R. T. Cederwall, and M. Zhang (2004), Developing long-term single-column model/cloud system–resolving model forcing data using numerical weather prediction products constrained by surface and top of the atmosphere observations, *J. Geophys. Res.*, *109*, D01104, doi:10.1029/2003JD004045.

Xie, S., S. A. Klein, M. Zhang, J. J. Yio, R. T. Cederwall, and R. McCoy (2006), Developing large-scale forcing data for single-column and cloud-resolving models from the Mixed-Phase Arctic Cloud Experiment, *J. Geophys. Res.*, *111*, D19104, doi:10.1029/2005JD006950.

Xie, S., T. Hume, C. Jakob, S. A. Klein, R. B. McCoy, and M. Zhang (2010a), Observed large-scale structures and diabatic heating and drying profiles during TWP-ICE, *J. Clim.*, *23*(1), 57–79, doi:10.1175/2009jcli3071.1.

Xie, S., et al. (2010b), Clouds and more: ARM Climate Modeling Best Estimate Data, *Bull. Am. Meteorol. Soc.*, *91*(1), 13–20, doi:10.1175/2009BAMS2891.1.

Xie, S., Y. Zhang, S. E. Giangrande, M. P. Jensen, R. McCoy, and M. Zhang (2014), Interactions between cumulus convection and its environment as revealed by the MC3E Sounding Array, *J. Geophys. Res. Atmos.*, *119*, 11,784–11,808, doi:10.1002/2014JD022011.

Xu, K.-M., et al. (2002), An intercomparison of cloud-resolving models with the atmospheric radiation measurement summer 1997 intensive observation period data, *Q. J. R. Meteorol. Soc.*, *128*(580), 593–624, doi:10.1256/003590002321042117.

Xu, K.-M., et al. (2005), Modeling springtime shallow frontal clouds with cloud-resolving and single-column models, *J. Geophys. Res.*, *110*, D15S04, doi:10.1029/2004JD005153.

Zhang, G. J., and N. A. McFarlane (1995), Sensitivity of climate simulations to the parameterization of cumulus convection in the Canadian climate centre general circulation model, *Atmos. Ocean*, *33*(3), 407–446, doi:10.1080/07055900.1995.9649539.

Zhang, J., et al. (2011), National Mosaic and Multi-Sensor QPE (NMQ) system: Description, results, and future plans, *Bull. Am. Meteorol. Soc.*, *92*(10), 1321–1338, doi:10.1175/2011bams-d-11-00047.1.

Zhang, M., and J. Lin (1997), Constrained variational analysis of sounding data based on column-integrated budgets of mass, heat, moisture, and momentum: Approach and application to ARM measurements, *J. Atmos. Sci.*, *54*(11), 1503–1524, doi:10.1175/1520-0469(1997)054<1503:CVAOSD>2.0.CO;2.

Zhang, M., J. Lin, R. T. Cederwall, J. J. Yio, and S. C. Xie (2001), Objective analysis of ARM IOP data: Method and sensitivity, *Mon. Weather Rev.*, *129*(2), 295–311, doi:10.1175/1520-0493(2001)129<0295:OAOAID>2.0.CO;2.